[7]Josyula, E., "Computational Study of Vibrationally Relaxing Gas Past Blunt Body in Hypersonic Flows," *Journal of Thermophysics and Heat Transfer*, Vol. 14, No. 1, 2000, pp. 18–26.

View-Factor-Based Radiation Transport in a Hypersonic Shock Layer

Deepak Bose* and Michael J. Wright†
NASA Ames Research Center,
Moffett Field, California 94035

Introduction

ATOMS and molecules in the hot shock layer formed in front of a hypersonic vehicle often release some of their internal energy by spontaneous emission of electromagnetic radiation. The isotropically emitted radiative energy propagates through the shock layer, sometimes undergoing absorption, until a portion of the remaining energy eventually reaches the body surface and heats the vehicle. In cases of high-speed entries of large vehicles, the radiative heating can be larger than the convective heating from the hot gas. It is therefore crucial to the design of the protective heat shield that this radiative-transport process be modeled accurately.

In practice radiative transport is typically reduced to a one-dimensional line-of-sight problem by assuming small body curvature and small tangential flow gradients. This approach is known as the tangent slab model. In this Note, we present a three-dimensional transport model based on geometric view factors between the emitting volumes and surface elements, which significantly improves the accuracy of radiative heat-flux estimates for an optically thin shock layer. This method can also be applied to absorbing gases, but the cost can be significantly more than the tangent slab model if fine spectral resolution is required.

Methodology

Shocklayer radiation is usually computed by assuming that it is uncoupled from the fluid dynamics. In this approach, the flowfield around the vehicle body is first simulated on a computational grid using a computational fluid dynamics (CFD) technique. The emission intensity $I_i(\nu)\,\mathrm{d}\nu$ W/m^3, where ν is the emission frequency, is then obtained at each computational cell i using known species densities and temperatures. The intensity can be computed using a full line-by-line method[1] or by using approximate band models. Assuming isotropic propagation, the radiative heat flux as a result of emission from the computational cell i with volume ΔV_i, to a surface element j with surface area ΔA_j (see Fig. 1) is written as[2]

$$\Delta q_{ij} = b_{ij} \int \frac{I_i(\nu)\Delta V_i}{\Delta A_j}\left(\frac{\Delta A_j \cos\theta_{ij}}{4\pi r_{ij}^2}\right)\tau(r_{ij},\nu)\,\mathrm{d}\nu \qquad (1)$$

where r_{ij} is defined in Fig. 1 as the distance between the center of the emitting volume and the center of the target area and θ_{ij} is the angle between the line of sight and the surface normal. The term

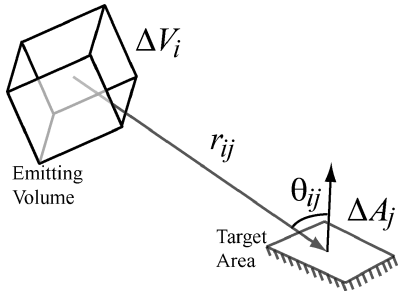

Fig. 1 Schematic of the line of sight and the relevant angle used in the view factor definition.

$\tau(r_{ij},\nu)$ is the attenuation factor caused by absorption in the gas and assumes a value of one for the optically thin case. The binary operator b_{ij} accounts for shadowing (caused by obstruction) effects that can arise for bodies with concave curvature; $b_{ij}=0$ if the line of sight intersects another portion of the surface prior to intersecting the target element and $b_{ij}=1$ otherwise. The computation of shadowing greatly increases the cost of the view factor algorithm and is not necessary for convex bodies. The areas on the back side of a convex body that does not see the radiation are eliminated as target elements because of a negative view factor ($\cos\theta_{Ij}<0$). Therefore, the binary operator b_{ij} is used only when a portion of the vehicle has a concave curvature, for example, vehicles with control surfaces.

The geometric view factor, defined as[2] $\Delta A_j \cos\theta_{ij}/4\pi r_{ij}^2$, is the fraction of radiative power that reaches the target surface element in the absence of absorption. The total radiative heat flux on surface element j is computed by summing over all emitting volumes:

$$q_j = \sum_i \Delta q_{ij} \qquad (2)$$

The validity of Eq. (1) rests on the assumption that dimensions of the emitting volume and the target area are much smaller than the distance between them. However, this condition is frequently violated in typical flowfield simulations because the thickness of the hot emitting layer between the shock and the body can be small enough that the cell dimensions are comparable to this thickness. Simply using Eq. (1) in such a case can yield unrealistically large view factors. This suggests that further refinement of the CFD grid is needed to compute the radiative transport. Therefore we divide the computational cells and the surface elements into smaller equal sized subcells. Each of these subcells has the same unit intensity as the original, but the view factors are different. If the emitting cell i is divided into m_0 subcells and the target surface element j into n_0 subelements, the modified radiative heat flux can be written as

$$\Delta q_{ij} = b_{ij} \int I_i(\nu)\frac{\Delta V_i}{\Delta A_j}\frac{1}{n_0 m_0}\sum_{m,n}\left(\frac{\Delta A_j \cos\theta_{imjn}}{4\pi r_{imjn}^2}\right)\tau(r_{imjn},\nu)\,\mathrm{d}\nu \qquad (3)$$

Strictly speaking, the number of subcells must be large enough to ensure that the resulting cell dimensions are much smaller than r_{ij}. However, near-wall cells (small r_{ij}), which would require the most subdivisions, are typically weakly emitting and do not contribute significantly to the radiative heating. Therefore in practice the cells are subdivided only until the change in predicted radiative heating is small.

Spherical-Cap Shock Layer

As an example, an analytical solution for radiative transport can be obtained for an optically thin hemispherical shock layer formed over a hemispherical body, as shown in Fig. 2. First, if we assume that radiation intensity I is constant over the shock layer of thickness Δr, we obtain the radiative heat flux at the stagnation point by integrating over the shock layer using the view factors to be

$$q_{\mathrm{vf}} = (I\Delta r/2)\left[\left(1-\sqrt{1-\beta^2}\right)/\beta^2\right], \qquad \beta = r_b/r_s \qquad (4)$$

Received 5 March 2004; revision received 4 June 2004; accepted for publication 7 June 2004.

*Senior Research Scientist, ELORET Corporation, Mail Stop 230-3. Member AIAA.

†Senior Research Scientist, Reacting Flow Environments Branch. Senior Member AIAA.

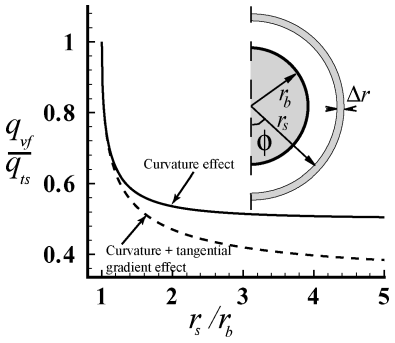

Fig. 2 Variation of the correction factor with shock radius normalized by the body radius. Schematic of the spherical-cap shock layer (inset).

where r_b and r_s are the radii of the body and shock, respectively. The tangent slab model ignores curvature, resulting in a stagnation-point heat-flux prediction of $q_{\text{ts}} = I\,\Delta r/2$. The additional factor in brackets in Eq. (4) is thus seen to be purely caused by curvature effects.

Now, let us introduce a tangential gradient of the radiation intensity along the shock by assuming that $I = I_0 \sin\varphi$, where I_0 is the peak intensity along the stagnation streamline ($\varphi = 90$ deg). In this configuration the view-factor-based heat flux is found to be

$$q_{\text{vf}} = \frac{I_0 \Delta r}{2}\left[\frac{(2+\beta^3) - \sqrt{1-\beta^2}(2+\beta^2)}{3\beta^3}\right] \tag{5}$$

However, for the tangent slab model we ignore the tangential gradient along with the curvature, which results in a prediction of $q_{\text{ts}} = I_0 \Delta r/2$ at the stagnation point. In this case the additional factor in brackets in Eq. (5) is caused by both the curvature and the tangential gradient in the shock layer. Figure 2 shows that the correction factor (defined as the ratio of the heat-flux values from the view factor method to the tangent slab method) decreases as the shock radius r_s increases with respect to the radius of the body for both cases expressed in Eqs. (4) and (5). We find that even for a small shock standoff distance with $r_b = 0.9 r_s$, q_{vf} is 30% smaller than q_{ts} purely as a result of curvature effects. When the tangential gradient is included, there is only an additional 0.8% drop in the heat flux. Therefore, the tangential gradient effects are very small compared to the curvature effect when the shock is close to the body. However, in the limit of a large shock standoff distance, $r_s \gg r_b$, the view-factor-based heat flux is half of the tangent slab value as a result of curvature effects, and only one-third of the tangent slab value when the tangential gradient is also considered. Although these estimates assume a sine variation of the intensity along the shock wave, the conclusions drawn herein are likely to be valid in realistic shock layers.

Titan Aeroshell Heating

An aerothermal analysis of a Titan aerocapture mission being considered by NASA[3] shows that the vehicle heating is dominated by cyanogen (CN, violet and red) radiation produced in the optically thin nitrogen-methane shock layer.[4] The proposed vehicle is a 3.75-m-diam 70-deg sphere cone that would enter at 6.5 km/s with a 16-deg angle of attack. In this Note, we demonstrate the improvement in the prediction of forebody radiative heat fluxes when the view-factor method rather than the tangent-slab model is used. Details of the previous aerothermal analysis can be found in Refs. 4 and 5. The view-factor-based heating is obtained using Eqs. (2) and (3). Each CFD computational cell and surface cell was divided into nine equal subcells, which was found to be sufficient to ensure a grid-converged result. The tangent-slab heat flux was computed along a line of sight normal to the body surface.

Figure 3 shows radiative heating on the pitch plane of this vehicle at the peak heating point computed with the view-factor and tangent-slab methods. The results show that the highest radiative heating on the forebody occurs on the wind side near the stagnation point. Figure 4 shows the correction factor $q_{\text{vf}}/q_{\text{ts}}$ on the body surface. We

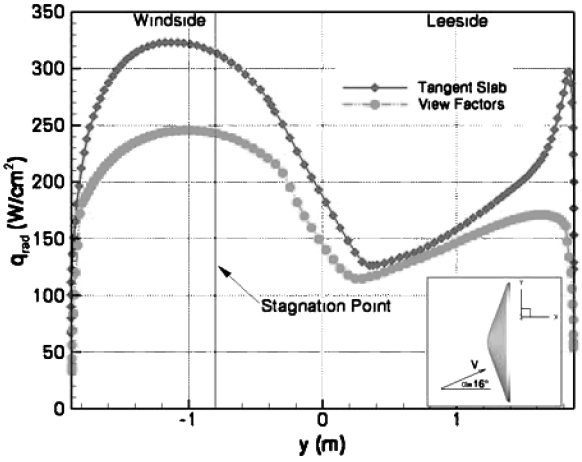

Fig. 3 Comparison of radiative heating on pitch plane of a Titan aerocapture vehicle computed with tangent-slab and the view-factor methods.

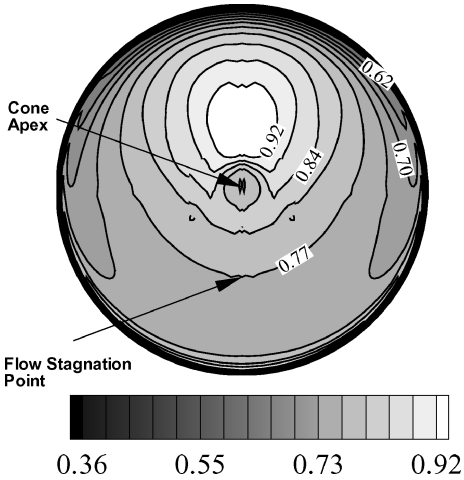

Fig. 4 Contours of the correction factor $q_{\text{vf}}/q_{\text{ts}}$ on the forebody of a Titan aerocapture vehicle.

find that the tangent-slab approach overpredicts the radiative heating by almost 32% in the stagnation region. This figure also shows that the correction factor is fairly constant (~0.74–0.80) on the entire wind side of the vehicle forebody, whereas on the lee side it stays closer to 1 (0.8–0.95). The tangent-slab approach is more applicable on the lee side because the shock standoff distance is smaller and the curvature is less.[4] The view-factor method makes the largest correction in the shoulder region as a result of sharp curvature and larger intensity gradients.

We observe that the correction factor is always less than unity on the forebody. For the spherical cap example discussed in the last section, the stagnation-point correction factor varies from 0.5–1 for zero-gradient shock layer and 0.33–1 when a tangential gradient is imposed. Although, in principle, a correction factor greater than one can be possible away from the stagnation point, this circumstance is unlikely to occur on a blunt forebody because the tangential gradients are usually small. It takes slightly more than an hour to complete a view-factor calculation for a grid with 1800 surface elements and 124,000 emitting volumes, whereas the tangent-slab method only takes about a minute, both on an Intel Xeon processor.

Summary

In summary, the results show that the use of tangent slab with an appropriate correction factor is a reasonable design choice in the stagnation region. However, the tangent-slab approximation can be extremely conservative in the shoulder region, where the underlying assumptions are violated. Also, radiative heating on the afterbody,

where the shock does not conform to the shape of the surface, is likely to be poorly predicted if the tangent-slab model is used.

Acknowledgment

The work performed by Bose is supported by the prime contract NAS2-99092 to ELORET.

References

[1]Whiting, E. E., Yen, L., Arnold, J. O., and Paterson, J. A., "NEQAIR96, Nonequilibrium and Equilibrium Radiative Transport and Spectra Program: User's Manual," NASA RP-1389, Dec. 1996.

[2]Hottel, H. C., and Sarofim, A. F., *Radiative Transfer*, McGraw–Hill, New York, 1967, p. 258.

[3]Lockwood, M., "Titan Aerocapture Systems Analysis," AIAA Paper 2003-4799, July 2003.

[4]Olejniczak, J., Prabhu, D., Wright, M., Takashima, N., Hollis, B., Sutton, K., and Zoby, V., "An Analysis of the Radiative Heating for Aerocapture at Titan," AIAA Paper 2003-4953, July 2003.

[5]Takashima, N., Hollis, B., Olejniczak, J., Wright, M., and Sutton, K., "Preliminary Aerothermodynamics of Titan Aerocapture Aeroshell," AIAA Paper 2003-4952, July 2003.

Finite Element Simulation of Radiative Heat Transfer in Absorbing and Scattering Media

L. H. Liu*

Harbin Institute of Technology, 150001 Harbin, People's Republic of China

Introduction

NUMERICAL solutions of the radiative-transfer equation in an absorbing, emitting, and scattering medium require considerable effort in most practical systems filled with semitransparent media. Recently, many numerical methods have been developed to solve the problem of radiative heat transfer in semitransparent media, for example, Monte Carlo method, zonal method, discrete ordinates method, spherical harmonics method, diffusion approximation, finite element method (FEM), and so on.

FEM has the following advantages: 1) the approximation for the field variables in a volume or surface element can vary across the element, and 2) the variation of field variables in the FEM can be specified to increase degrees of approximation. Because of its advantage, FEM was used by many researchers to solve the problems of radiative heat transfer in semitransparent media. Razzaque et al.[1] studied the finite element solution of radiative heat transfer in a two-dimensional rectangular enclosure with gray participating media. Lin[2] developed formal integral equations describing radiative transfer in an arbitrary isotropically scattering medium enclosed by diffuse surfaces. Anteby et al.[3] used FEM to calculate the combined conduction and radiation transient heat transfer in a semitransparent medium. Furmanski and Bannaszek[4] applied FEM to solve the coupled conduction and radiation heat transfer in participating media. The conventional finite element simulations for radiative heat transfer are all based on the concept similar to zone method, in which the incoming intensity or source function is formulated as a formal integration by relating it to all surface and volume elements. Therefore, very complex geometrical integration was needed, especially for the problem of multidimensional irregular geometry.

Based on the discrete-ordinate equations of radiative transfer, Fiveland and Jessee[5] developed a finite element formulation of discrete-ordinates method for multidimensional geometries, in which the even parity radiative transfer equation is formulated for an absorbing, isotropically scattering, and reemitting medium enclosed by gray walls. The even parity radiative-transfer equation is a second-order form of transport equation, and hence the complex geometrical integration is avoided in finite element simulation. However, the even parity radiative transfer equation used by Fiveland and Jessee[5] is derived from the assumption of isotropically scattering, and cannot be used for anisotropically scattering media.

In this Note, to avoid the complex geometrical integration and consider the anisotropically scattering we develop a finite element formulation of radiative transfer based on the original discrete-ordinate equations. Two cases of radiative heat transfer in two-dimensional rectangular enclosure filled by semitransparent media are examined to verify this new formulation.

Mathematical Formulation

Consider the radiative transfer in the enclosure filled with semitransparent media. The discrete-ordinate equations of radiative transfer can be written as[6,7]

$$\mu_m \frac{\partial I^m}{\partial x} + \eta_m \frac{\partial I^m}{\partial y} + \xi_m \frac{\partial I^m}{\partial z} = -(\kappa+\sigma) I^m + \kappa I_b + \frac{\sigma}{4\pi} \sum_{m'=1}^{M} I^{m'} \Phi^{m'm} w' \tag{1}$$

with boundary conditions

$$I_w^m = \varepsilon_w I_{bw} + \frac{1-\varepsilon_w}{\pi} \sum_{|n_w \cdot s_{m'}|<0} I_w^{m'} |\boldsymbol{n}_w \cdot \boldsymbol{s}_{m'}| w_{m'} \tag{2}$$

where I^m is the radiation intensity at the direction m; I_b is the intensity of blackbody radiation at the temperature of the medium; κ and σ are the absorption and scattering coefficients of the medium, respectively; Φ is the scattering phase function; ε_w is the wall emissivity; $\boldsymbol{n}_w$ is the unit normal vector of boundary surface; $\boldsymbol{s}_{m'}$ is the unit vector in the direction m'; μ_m, η_m, and ξ_m are the direction cosine; and w_m is the weight corresponding to the direction m. By removing the forward scattering from right side of Eq. (1) to the left side, Eq. (1) can be rewritten as[8]

$$\mu_m \frac{\partial I^m}{\partial x} + \eta_m \frac{\partial I^m}{\partial y} + \xi_m \frac{\partial I^m}{\partial z} + \left(\kappa + \sigma - \frac{\sigma}{4\pi}\Phi^{mm} w\right) I^m = \kappa I_b + \frac{\sigma}{4\pi} \sum_{m'=1, m' \neq m}^{M} I^{m'} \Phi^{m'm} w', \qquad m = 1, 2, \ldots, M \tag{3}$$

By using the shape function, an approximate solution of I^m is assumed in the form

$$I^m = \sum_{l=1}^{N} I_l^m \varphi_l \tag{4}$$

where the I_l^m is the values at the node l and φ_l is the shape function. The weighted residuals approach is used to spatially discretize the discrete ordinate equations [Eq. (3)]. Taking shape function φ_l as the weight function, Eq. (3) is weighted over the domain of interest

Received 17 May 2004; revision received 4 July 2004; accepted for publication 6 July 2004.

*Professor, School of Energy Science and Engineering, 92 West Dazhi Street; lhliu@hit.edu.cn.